



PII S0016-7037(00)00366-5

Genesis of the Mars Pathfinder “sulfur-free” rock from SNC parental liquids

M. E. MINITTI* and M. J. RUTHERFORD

Department of Geological Sciences, Brown University, Providence, RI 02912, USA

(Received September 21, 1999; accepted in revised form March 1, 2000)

Abstract—Combined rock and soil measurements from the Mars Pathfinder APXS established the composition of the “sulfur-free” rock whose chemical characteristics suggest it is an igneous andesite. We experimentally investigated the formation of the sulfur-free rock through equilibrium crystallization of a primitive SNC basalt under hydrous (1.0–1.5 wt% H₂O) and dry conditions at the QFM oxygen buffer. The experiments determined crystallization sequences and liquid lines of descent for a basalt with a high-FeO, low-Al₂O₃ (relative to tholeiitic magma) composition characteristic of SNC magmas. In the hydrous experiments, the crystallization sequence between ~1090°C and 950°C is pigeonite → sub-calcic augite → Ti-magnetite → plagioclase → ilmenite + fayalite. The crystallization sequence of dry experiments between ~1130°C and 980°C resembles that of the hydrous experiments except for the appearance of plagioclase and fayalite before Ti-magnetite. The liquid lines of descent reveal that fractionation of a hydrous, primitive SNC basalt can produce a melt equivalent to the sulfur-free rock composition whereas fractionation of a dry SNC basalt fails to produce such a melt. The effect of water on the timing and amount of phenocryst growth, particularly Fe-Ti oxide crystallization, is critical in achieving the observed SiO₂ enrichment in the hydrous experiments. The hydrous basalt reaches andesitic residual melt compositions at ~40% crystallization and the dry basalt eventually produces a minimum andesitic composition melt at ~90% crystallization. The low degree of crystallization necessary to reach andesitic residual melt compositions in the hydrous experiments would greatly facilitate the extraction of this andesitic melt (and more evolved melts) from associated crystals. Further experiments at other oxygen fugacities reveal that oxidizing fO₂'s (MnO-Mn₃O₄) encourage silicic melt formation by enhancing oxide crystallization; conversely, reducing fO₂'s (GCH) hinder silicic melt formation. By analogy with terrestrial magmatic processes, water could enter basaltic melt on Mars through one or more pathways: partial melting of water-bearing mantle and concentration of water by fractional crystallization; stopping or assimilation of hydrothermally altered crust; direct introduction of hydrothermal fluids into a magma during caldera collapse. *Copyright © 2000 Elsevier Science Ltd*

1. INTRODUCTION

The study of Martian rocks has largely been limited to the SNC meteorites, a group of 14 achondrites including basalts, microgabbros, pyroxenites and a dunite, whose parent body is widely accepted as Mars. The Mars Pathfinder mission provided a new opportunity to directly study rocks from the Martian surface in light of the knowledge gained from the Viking missions and from the SNC meteorites. Five rock and six soil samples were analyzed by the APXS on Mars Pathfinder and compositions of rocks and soils from the x-ray portion of the APXS spectra were reported by Rieder et al. (1997). When the Pathfinder soil and rock data are plotted on oxide vs. sulfur (S) diagrams, they define reasonably linear arrays across a range of S contents, with soils falling at consistently higher S contents (Rieder et al., 1997). The solubility of S in basaltic melts is low (≤ 0.3 wt%; Carroll and Webster, 1994) in comparison to the rock analyses, implying that the range of S contents in the rock analyses results from incorporation of differing amounts of soil component in each rock analysis. This suggestion is confirmed by camera images which show variable dust coatings on the rocks of the Pathfinder landing site and by spectral analyses of rocks that are best fit by mixtures of rock and soil (McSween et al., 1999). The rock compositions all lie on a mixing line between the soils and a

hypothetical “sulfur-free” rock obtained by extrapolating a regression line through the rock data back to 0 wt% S (Rieder et al., 1997).

The classification of the sulfur-free rock as igneous, sedimentary, metamorphic or impact-derived is a subject of debate, but several chemical arguments exist in favor of an igneous origin. The sulfur-free rock shares low-Al₂O₃ and high-FeO contents (McSween et al., 1999) in common with the SNC meteorites, which are all igneous rocks. The sulfur-free rock also falls on the Mars mantle-crust fractionation line which is delineated by the SNC meteorites (Rieder et al., 1997). Additionally, compositions of all the rocks measured at the Pathfinder landing site fall along a tholeiitic fractionation trend on an AFM diagram (McSween et al., 1999). Terrestrial andesites formed along a tholeiitic differentiation trend are associated with the low-pressure crystallization of basaltic parent liquids, as occurs in Iceland (Carmichael, 1964) or the Galapagos Spreading Center (Spulber and Rutherford, 1983). Finally, when the CIPW norm of the sulfur-free rock is calculated, it consists of hypersthene, diopside, feldspars and quartz in proportions found in terrestrial igneous rocks (McSween et al., 1999). If the sulfur-free rock is an igneous rock, its SiO₂ and alkali content classify it as an andesite (McSween et al., 1999).

Assuming that the Pathfinder sulfur-free rock is igneous, McSween et al. (1999), considered possible origins for a magma of this composition. First, they calculated a liquid line of descent (residual melts) produced by dry crystallization of

* Author to whom correspondence should be addressed (Michelle_Minitti@brown.edu).

Table 1. Important melt and rock compositions.

Oxide	Shergotty ^a	Chassigny ^b	Nakhla ^c	EETA79001 ^d	GSC Basalt ^e	A* ^f	A*-2 ^g	S-free Rock ^h
SiO ₂	50.8	51.52	50.2	49.20	51.35	50.33	51.38	62.0 ± 2.7
Al ₂ O ₃	8.0	8.72	8.6	6.44	13.21	8.16	7.71	10.6 ± 0.7
FeO*	19.8	19.02	19.1	18.49	13.43	19.87	19.71	12.0 ± 1.3
MgO	7.7	7.08	4.0	14.40	6.12	7.39	7.27	2.0 ± 0.7
CaO	9.7	8.49	11.9	7.96	10.74	8.95	9.76	7.3 ± 1.1
Na ₂ O	1.5	2.29	1.2	0.97	2.3	1.71	1.52	2.6 ± 1.5
K ₂ O	0.2	0.77	2.8	0.06	0.1	0.43	0.33	0.7 ± 0.2
TiO ₂	1.0	1.58	1.0	0.78	2.14	1.75	0.96	0.7 ± 0.1
P ₂ O ₅	0.9	—	0.7	—	0.18	0.5	0.62	0.8 ± 0.2
MnO	0.5	0.53	0.4	0.51	na	0.52	0.54	na

^a From Hale et al. (1999): intercumulus melt composition.

^b From Johnson et al. (1991): trapped melt composition.

^c From Treiman (1993): trapped melt composition; does not include 0.1 wt% Cr₂O₃.

^d From McSween and Jarosewich (1983): parental melt composition.

^e From Juster et al. (1989): Galapagos Spreading Center FeTi basalt composition.

^f Fusion glass composition (P = 1 atm, T = 1300 C, time = 4 hours, in Mo foil).

^g Fusion glass composition (P = 1 atm, T = 1300 C, time = 4 hours, in Mo foil).

^h From Rieder et al. (1997) and T. Economou (personal comm., 1999).

the early (high MgO) intercumulus basaltic melt in Shergotty (Hale et al., 1999; Table 1) using the MELTS program (Ghiorsso and Sack, 1995). They found that the liquid line of descent did not lead to the sulfur-free rock composition and they concluded that SNC basaltic magmas could not produce melts equivalent to the analyzed rocks of the Pathfinder landing site under dry, low-pressure conditions. Second, they applied an experimental liquid line of descent which reproduces Galapagos andesitic liquids (Juster et al., 1989) to the sulfur-free rock composition. McSween et al. (1999) reported that the experimentally determined Galapagos liquid line of descent formed by fractional crystallization of a dry Galapagos basalt successfully reproduces many of the compositional characteristics of the sulfur-free rock. They concluded that water was not required for formation of the sulfur-free rock and suggested that the sulfur-free rock might have had a more aluminous, terrestrial-like parent. It should be noted that the Galapagos basalt from which Juster et al. (1989) derive their liquid line of descent, while higher in FeO and generally lower in Al₂O₃ relative to other terrestrial basalts, does not have the high-FeO content and low-Al₂O₃ contents characteristic of SNC basalts (Table 1).

Crystallization of dry basalt is not the only pathway by which andesites form. Studies of terrestrial rocks indicate that water is commonly involved both in the production of island arc andesites and in production of andesitic magmas in ocean island settings such as Iceland (Gunnarsson et al., 1998). Water has a known and significant effect on phase equilibria of crystallizing melts. Water depolymerizes the melt by breaking Si-O-Si bonds, making it more difficult for polymerized silicates, especially plagioclase, to crystallize (Spulber and Rutherford, 1983). While the presence of dissolved water in the melt lowers the crystallization temperature of silicates, it has little effect on Fe-Ti oxide crystallization. As a result, Fe-Ti oxides appear early in the crystallization sequence of a water-bearing basalt. The effect of water is illustrated by the differences in the behavior of Al₂O₃ and FeO along the liquid lines of descent of hydrous and anhydrous experiments on a Galapagos Spreading Center basalt (Fig. 1). The dry liquid line of descent (LLD) is

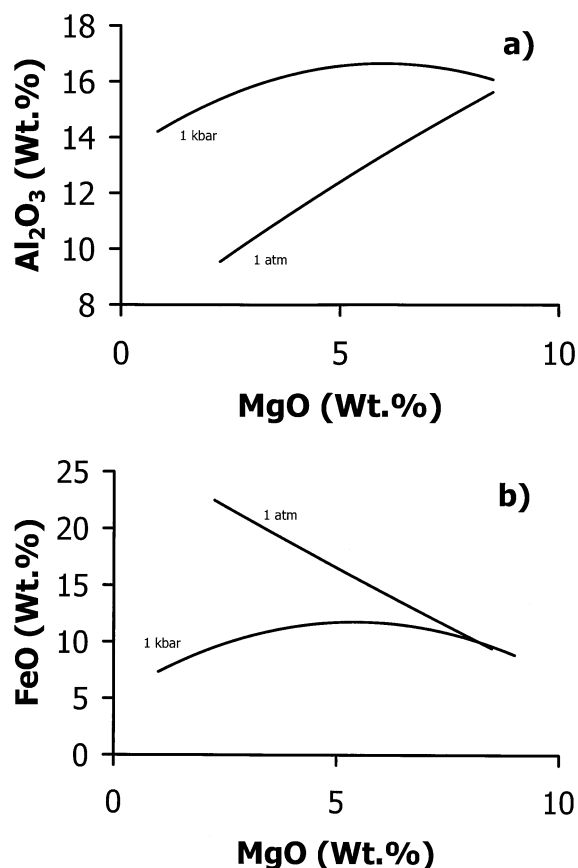


Fig. 1. Liquid lines of descent for a Galapagos Spreading Center tholeiitic basalt under dry and hydrous conditions from Spulber and Rutherford (1983). The individual liquid lines of descent are labeled with the total pressure of each experiment. The 1 atm experiment is anhydrous and the $P_{\text{total}} = 1$ kbar experiment has $P_{\text{H}_2\text{O}} = 670$ bars. (a) Al₂O₃ vs. MgO. In a dry melt, early plagioclase crystallization leads to an early decrease in melt Al₂O₃. In a hydrous melt, delayed plagioclase crystallization allows melt Al₂O₃ to increase until the eventual crystallization of plagioclase. (b) FeO vs. MgO. In a dry melt, Fe-Ti oxides crystallize late, thus allowing melt FeO to build in concentration. In a hydrous melt, Fe-Ti oxides crystallize early which leads to decreases in melt FeO.

Table 2. Summary of experiments.

Run	Starting material	$T_i - T_f$ (C)	P_{total} (bars) ^a	Hours at T_f	fO_2 ^b	Products ^{c,d}
MS-18	MS-2	1089 – 1089	200	38	QFM	gl + pig
MS-3	A* powder	1075 – 1075	200	24	QFM	gl + pig + aug
MS-25	MS-19	1075 – 1075	200	100	QFM	gl + pig + aug
MS-28	MS-19	1100 – 1060	200	24	QFM	gl + pig + aug
MS-33	MS-30	1060 – 1060	200	57	QFM	gl + pig + aug
MS-1	A* powder	1050 – 1050	200	24	QFM	gl + pig + aug + mag
MS-38r	MS-6	1050 – 1050	200	48	QFM	gl + pig + aug + mag
MS-2	A* powder	1057 – 1025	200	15	QFM	gl + pig + aug + mag + plag
MS-6	A* powder	1050 – 1000	200	12	QFM	gl + pig + aug + mag
MS-30	MS-28	1050 – 975	200	70	QFM	gl + pig + aug + mag + ilm + plag
MS-51	A* powder	950 – 950	200	55	QFM	gl + pig + aug + mag + ilm + plag + ol
MS-19	A* powder	1130 – 1130	1	32	QFM	gl + pig
MS-70	A*-2 Glass	1080 – 1080	1	96	QFM	gl + pig + aug + plag
MS-68	MS-59	1065 – 1065	1	96	QFM	gl + pig + aug + plag + ol
MS-59	MS-52	1050 – 1050	1	192	QFM	gl + pig + aug + mag + plag + ol
MS-56	MS-50	1050 – 1050	1	96	QFM	gl + pig + aug + mag + ol
MS-45	A* Glass	1030 – 1030	1	216	QFM	gl + pig + aug + mag + plag + ol + ilm
MS-52	MS-45	1030 – 980	1	156	QFM	gl + pig + aug + mag + plag + ol + ilm
MS-60	A* Glass	1030 – 1030	100	96	QFM	gl + pig + aug + mag
MS-72	A*-2 Glass	1030 – 1030	200	24	GCH	gl + pyx + plag + FeTi
MS-73	A*-2 Glass	1030 – 1030	200	24	MNO	gl + pyx + FeTi + plag + qtz

^a $P_{\text{total}} = P_{\text{H}_2\text{O}}$.

^b QFM: Quartz-fayalite-magnetite buffer.

GCH: Graphite-methane buffer.

MNO: MnO – Mn₃O₄ buffer.

^c gl = glass, pig = pigeonite, aug = sub-calcic augite, mag = Ti-bearing magnetite, ilm = ilmenite, ol = Fe-rich olivine, plag = plagioclase.

^d Specific phase compositions were not determined for the products MS-60, MS-72 and MS-73. Phases identified petrographically or through EDS on the electron microprobe are: gl = glass, pyx = pigeonite and/or augite, plag = plagioclase, FeTi = Fe-Ti oxides, qtz = quartz.

characterized by a steady decrease in Al₂O₃ (Fig. 1a) due to early crystallization of plagioclase. In contrast, the hydrous LLD shows an initial increase in Al₂O₃ due to the suppressed crystallization of plagioclase caused by water in the melt. After plagioclase crystallization begins, the melt Al₂O₃ decreases steadily (Fig. 1a). The dry LLD shows a steady increase in FeO (Fig. 1b) with decreasing MgO (temperature) because of the lack of early Fe-Ti oxide crystallization. FeO also builds in the hydrous melt before Fe-Ti oxides crystallize, but early Fe-Ti oxide crystallization in the hydrous experiment leads to decreases in melt FeO. Differences between the dry and hydrous basaltic LLD's are important when considering the formation of the Mars Pathfinder sulfur-free rock. The effect of water on basaltic liquid lines of descent may make it possible to derive this andesitic rock from a SNC basalt. The goal of this study is to investigate the formation of the sulfur-free rock from a primitive SNC basaltic parent, focusing on the potential role of water in the petrogenetic process.

2. EXPERIMENTAL AND ANALYTICAL

We have conducted experiments on A*, a primitive melt calculated to be in equilibrium with olivine and Ca-pyroxene in Chassigny (Johnson et al., 1991). Another starting material was also used (A*-2) which is slightly modified from A* (Table 1). Both compositions have the characteristic high-FeO and low-Al₂O₃ concentrations associated with Martian igneous rocks and they closely resemble other experimentally and theoretically determined SNC primitive melt compositions (Table 1), including the starting SNC magma composition used by McSween et al. (1999). Hydrous crystallization and melting experiments were conducted on either powdered or glassy (fused above the liquidus) A* starting material sealed in AgPd tubing. Experiments were also conducted on products of earlier experiments. This was done because it is

an effective way to achieve long run times and a closer approach to equilibrium, and it is the only way to “reverse” the approach to the equilibrium assemblage. Experiments were run at $P_{\text{total}} = P_{\text{H}_2\text{O}} = 200$ bars in TZM pressure vessels with Ar and CH₄ used as the pressurizing gases. A pressure of 200 bars was selected for the initial set of experiments in order to achieve ~1.5 wt% H₂O in the melt. This amount of water is consistent with the findings of SNC melt inclusion studies (e.g. Johnson et al., 1991) and is likely to affect the crystallization sequence according to previous experimental studies (e.g. Spulber and Rutherford, 1983). Melt water contents of 1.5 wt% were called into question by the studies of Watson et al. (1994) and Popp et al. (1995), but the potential effects of shock-induced water loss (Minitti et al., 1999) and post-crystallization dehydrogenation (King et al., 1999) in amphibole suggest that 1.5 wt% H₂O in the melt is still tenable in some SNC magmas. A pressure of 200 bars corresponds to approximately 1.5 km depth in the Martian crust. A single experiment was also conducted at $P_{\text{total}} = P_{\text{H}_2\text{O}} = 100$ bars and 1030°C in order to investigate the behavior of a basaltic magma with ~1.0 wt% H₂O. All experiments were buffered at an fO_2 equivalent to the QFM buffer using a combination of methods. First, the Ar and CH₄ used as the pressurizing gases were mixed in order to maintain approximately QFM conditions within the pressure vessel. Second, the sample tube was placed in a larger buffer tube containing powdered QFM buffer and water in order to maintain QFM oxygen fugacity immediately outside the experimental charge. The QFM buffer selection is based on fO_2 estimates from several SNC meteorites (e.g. Stolper and McSween, 1979). However, there is still some uncertainty about the range of oxygen fugacities recorded by the SNC meteorites (Ghosal et al., 1998; Delaney et al., 1998). One SNC sample, QUE94201, records an fO_2 of the IW buffer (McSween et al., 1996). Therefore, we also ran experiments at more reducing and oxidizing conditions (Table 2). Experimental temperatures, known to within ±8°, ranged between 1089°C and 950°C and run durations ranged between 24 and 100 hours.

We also investigated the crystallization of dry A* melt with a series of 1 atmosphere crystallization experiments. Powdered or glassy A* starting materials or the products of previous experiments were con-

tained in either AgPd or AuPd tubes which were then sealed in evacuated SiO₂ glass tubes. AgPd tubes were used at experimental temperatures (<1060°C) safely below the melting temperature of AgPd to minimize Fe loss from the experimental material. AuPd tubes were used at temperatures above the melting temperature of AgPd. The AuPd tubes were saturated with A* by filling them with A* powder and holding them at the experimental temperature. The tubing was saturated because of the tendency of AuPd to draw Fe from the sample at lower oxygen fugacities. All experiments were buffered using a QFM assemblage in an external, unsealed tube. Experimental temperatures ranged between 1130°C and 980°C and experiment durations ranged between 32 hours and 9 days (Table 2).

Major oxide analyses of the experimental products were conducted on the Brown University Cameca Camebax electron microprobe. Analysis conditions included a 15 kV accelerating voltage, a 10 nA defocused beam for glasses and a 15 nA focused beam for oxide and silicate analyses. Glasses were always analyzed first. During glass analyses, the electron beam was blanked between analyses and a Na loss program (Nielsen and Sigurdsson, 1974) was utilized to obtain Na₂O concentrations.

3. RESULTS

3.1. General

A description of the experiments including the phases produced in both the hydrous and dry experiments is presented in Table 2. The dry 1 atm liquidus for the A* composition is 1150°C; the hydrous 200 bar liquidus is 1095°C. The sequence of mineral crystallization in the hydrous experiments is pigeonite, sub-calcic augite, Ti-magnetite, plagioclase, ilmenite and fayalite. In the dry experiments, the crystallization sequence is pigeonite, sub-calcic augite, plagioclase, fayalite, Ti-magnetite and ilmenite. The crystals in all of these experiments ranged up to ~100 μm. Mineral and residual melt (glass) compositions determined by electron microprobe analysis were used in the PETMIX program (Wright and Doherty, 1970) to calculate the mode of each experiment (Fig. 2). The residual melt data were used to construct LLD's (Fig. 3). The LLD's we have determined are considered to represent near-equilibrium melt evolution paths. This means that after crystallizing the starting basalt at various temperatures, the crystal-melt assemblage at each temperature is essentially an equilibrium assemblage. Perfect equilibrium crystallization was not achieved because there is some variability (zoning) in pyroxene compositions especially in some of the lower temperature experiments. We tested for approach-to-equilibrium by conducting both crystallization and melting experiments at various temperatures. In the dry experiments, a single crystallization/melting experiment pair was carried out at 1050°C. The pair consistently have the same residual melt compositions within analytical uncertainty (Fig. 3), for all oxides, suggesting that the four day experiment durations were sufficient to achieve a close approach to equilibrium. In the suite of hydrous experiments, pairs of crystallization and melting experiments were attempted at 1060°C and 1050°C. The pair of experiments conducted at 1060°C have residual melt compositions identical within error (Fig. 3). This implies that equilibrium was achieved in the 1060°C experiments and that the pair of experiments effectively constrains the hydrous LLD. The 1050°C experiments do not bracket an intermediate composition but both fall along the LLD trend. The short duration of the 1050°C crystallization experiment might have affected the composition of the residual melt. The residual melt compositions of the two 1075°C crystallization

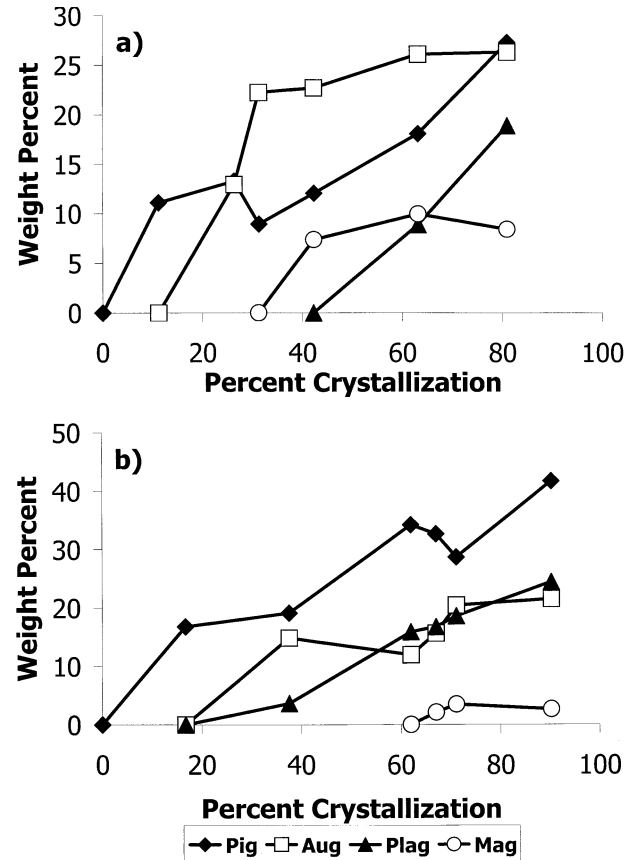


Fig. 2. Results of mode (weight percent) calculations of the experimental products conducted with the PETMIX program (Wright and Doherty, 1970). Mineral and glass compositions used in PETMIX were obtained through electron microprobe analyses. (a) Hydrous experimental products. The temperature of the hydrous liquidus (0% crystallization) is ~1095°C and the lowest temperature experiment (~80% crystallization) was conducted at 950°C. (b) Dry experimental products. The temperature of the dry liquidus (0% crystallization) is ~1150°C and the lowest temperature experiment (~90% crystallization) was conducted at 975°C.

experiments are somewhat different although both fall along the LLD trend. The difference likely results from extensive quench crystal formation. These melts proved difficult to quench from high temperatures because of their high-FeO, low-Al₂O₃ character. Similarly, the products of the 1089°C experiment, a melting experiment, contain pyroxene quench crystals. The quench crystals are Fe-rich relative to the well-formed pyroxenes and appear to have affected the composition of the 1089°C residual melt, leading to the overlap of residual melt compositions of the 1089°C experiment and one of the 1075°C experiments. While these experimental difficulties cause small shifts in residual melt compositions and the LLD at high temperatures, they do not affect the position of the LLD at lower temperatures.

3.2. Hydrous Phase Assemblage and LLD

The nature and the abundance of phases that crystallized in the 200 bar experiments is illustrated by the calculated modes (Fig. 2a) and products of typical experiments are shown in Fig.

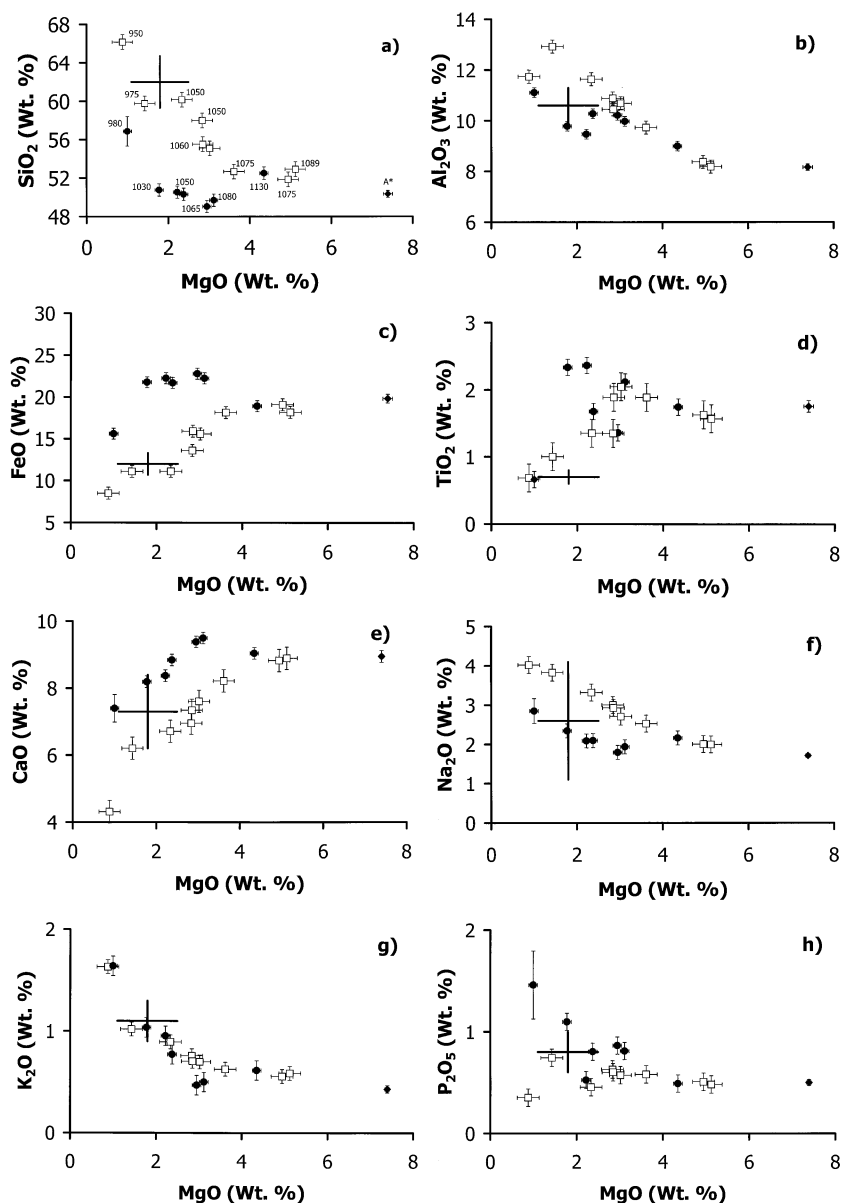


Fig. 3. Experimental data relative to the composition of the sulfur-free rock and the A* starting material. Open squares represent the hydrated data and filled circles represent the dry data. The diamond is A* and the cross is the sulfur-free rock. In all figures, degree of crystallization increases to the left. Error bars encompass $\pm 1\sigma$ for each data point. The sulfur-free rock composition is a recalibrated composition and the cross marking the sulfur-free rock composition delineates the analytical uncertainties in the APXS measurements reported by Brückner et al. (1999). (a) SiO₂ vs. MgO. Temperatures of the individual experiments are indicated next to the respective data point and are applicable throughout Fig. 3. The hydrated liquid line of descent (LLD) approaches the sulfur-free rock composition more closely than the one atmosphere LLD because of earlier oxide crystallization in the hydrated experiments. (b) Al₂O₃ vs. MgO. The dry and hydrated LLD's achieve the Al₂O₃ content of the sulfur-free rock despite different timing of plagioclase crystallization in the suites of experiments. (c) FeO vs. MgO. The hydrated LLD approaches the sulfur-free rock composition more closely than the dry LLD because of earlier oxide crystallization in the hydrated experiments. (d) TiO₂ vs. MgO. Earlier oxide crystallization in the hydrated experiments allows the hydrated LLD to approach the sulfur-free rock composition more closely than the dry LLD. (e) CaO vs. MgO. Different amounts of augite crystallization lead to different decreases in CaO in the hydrated and dry LLD's. The LLD's reproduce the CaO content of the sulfur-free rock with similar effectiveness. (f) Na₂O vs. MgO. The constant increases in melt Na₂O in both the dry and hydrated experiments indicate that Na₂O acted as an incompatible element throughout crystallization in all experiments. The dry and hydrated LLD's reach the Na₂O content of the sulfur-free rock. (g) K₂O vs. MgO. Just as with Na₂O, K₂O acted as an incompatible element across the experimental range investigated. The dry and hydrated LLD's overlap on their approach to the sulfur-free rock composition. (h) P₂O₅ vs. MgO. The P₂O₅ error bar is estimated at ± 0.2 wt% because no published error determinations are available. P₂O₅ increases with decreasing temperature in most of the hydrated experiments and in all of the dry experiments. The P₂O₅ content of the lowest temperature hydrated experiments decreased, indicating the formation of a P₂O₅-rich phase. The dry and hydrated LLD's reach the P₂O₅ content of the sulfur-free rock.

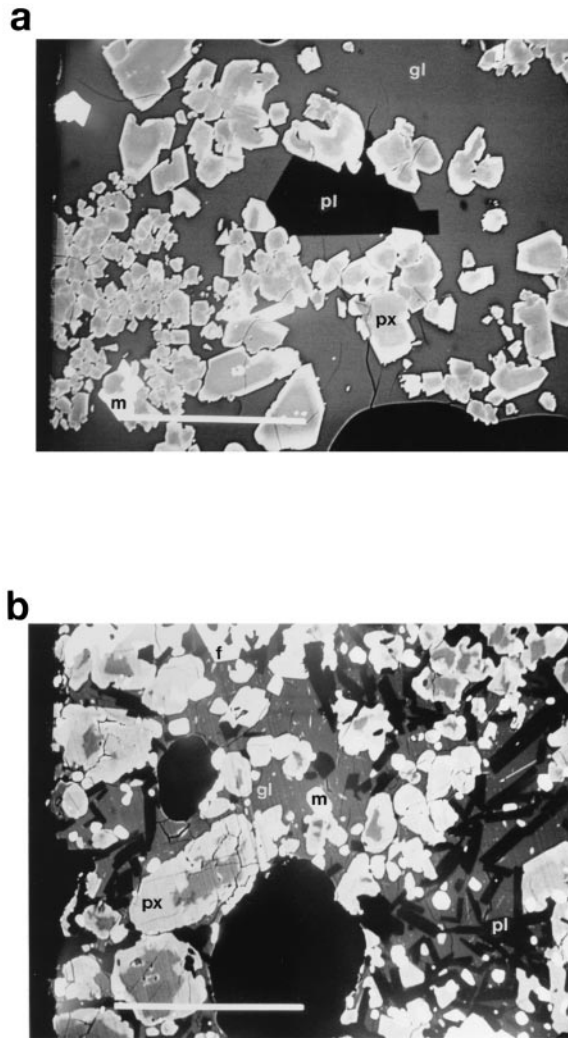


Fig. 4. Backscattered electron images of experimental products. Scale bar in both pictures is 100 μm . (a) Hydrous, 975°C experimental product (MS-30). Sub-calcic augite and pigeonite (px), plagioclase (pl) and Ti-magnetite (m) are present and are in contact with the glass (gl). Sub-calcic augite core to rim compositions vary between $\text{Wo}_{37}\text{En}_{43}\text{Fs}_{20}$ to $\text{Wo}_{36}\text{En}_{37}\text{Fs}_{26}$ and pigeonite core to rim pyroxene compositions vary between $\text{Wo}_{14}\text{En}_{56}\text{Fs}_{30}$ to $\text{Wo}_{13}\text{En}_{42}\text{Fs}_{45}$. (b) Dry, 980°C experimental product (MS-52). Pigeonite, sub-calcic augite and oxides are labeled as in (a) and fayalite is also pictured (f). Cores ($\text{Wo}_{27}\text{En}_{46}\text{Fs}_{26}$) are incompletely reacted remnant pyroxenes from the starting material. Rim pigeonite compositions reach $\text{Wo}_{16}\text{En}_{31}\text{Fs}_{52}$ and rim augite compositions reach $\text{Wo}_{33}\text{En}_{30}\text{Fs}_{37}$.

4a. From the liquidus ($\sim 1095^\circ\text{C}$) down to 1075°C , pigeonite ($\text{En}_{60}\text{Fs}_{30}\text{Wo}_{10}$) is the sole crystallizing phase. At 1075°C , a sub-calcic augite ($\text{En}_{42}\text{Fs}_{29}\text{Wo}_{29}$) joins pigeonite, and throughout the lower temperature experiments, some compositional zoning of pyroxenes is observed. Representative pyroxene compositions are pictured in Figure 5 relative to pyroxene compositions from the dry experiments and from the SNC meteorites. The pyroxenes of the hydrous experiments overlap the compositions of the SNC pyroxenes, particularly those of Shergotty (Hale et al., 1999). At 1050°C , Ti-bearing magnetite crystallizes and as the experimental temperatures decrease, the amount of TiO_2 within the magnetite increases. The two py-

roxenes and magnetite are joined by plagioclase ($\text{An}_{44}\text{Ab}_{55}\text{Or}_1$ to $\text{An}_{53}\text{Ab}_{46}\text{Or}_1$) and rare ilmenite at 975°C and below. No zoning is observed in the plagioclase grains. At 950°C , an Fe-rich olivine (Fo_{32}) joins the assemblage and no zoning is observed in the olivine crystals. Olivine does not appear on the liquidus because the A* melt has low-Ca pyroxene in reaction relationship with olivine (Johnson et al., 1991). Representative compositions of the crystallized minerals are given in Table 3.

For each experiment, a pure Fe phase was allowed into the mode calculations to investigate if Fe loss to or Fe gain from the capsule had occurred. PETMIX indicated that 2–3% Fe loss occurred in the three experiments at $\geq 1075^\circ\text{C}$ and in two lower temperature experiments ($\sim 1060^\circ\text{C}$) whose starting material was a one atmosphere experimental product that experienced Fe loss. In the cases where Fe loss was indicated, the percentages of phases calculated by PETMIX were renormalized to 100%. The effects of the Fe loss are small and do not affect any experiments on the LLD below 1060°C .

The compositions of the residual liquids in the experiments (Table 4) are plotted in Figure 3 relative to the A* basalt starting composition. As temperature decreases, the MgO contents of the residual melts continuously decrease. Thus, decreasing MgO is a good proxy for decreasing temperature. The SiO_2 contents of the residual melts in the hydrous experiments (Fig. 3a) undergo a small increase relative to the bulk A* melt prior to magnetite crystallization (1050°C). Once Ti-magnetite joins pigeonite and sub-calcic augite in the crystallizing assemblage, significant increases in melt SiO_2 occur with further decreases in temperature. The residual experimental melts reach andesitic SiO_2 contents shortly after Fe-Ti oxides begin to crystallize. Residual melt Al_2O_3 increases steadily through all but the lowest temperature experiments due to the combined crystallization of the Al_2O_3 -poor pyroxenes and magnetite (Fig. 3b). Melt Al_2O_3 decreases only at temperatures below 975°C when plagioclase is crystallizing. This behavior mimics the LLD for terrestrial basalt crystallization under hydrous conditions (Fig. 1a). The FeO content of residual melts decreases slightly during pyroxene-only crystallization, (Fig. 3c) but once magnetite saturation is achieved, the melt FeO decreases steadily throughout the experiments with decreasing temperature. The overall pattern of melt FeO resembles the hydrous liquid line of descent obtained from terrestrial basalts (Fig. 1b). The behavior of TiO_2 in the experimental glasses is similar to that of FeO, increasing initially as pyroxenes crystallize and decreasing upon magnetite (and later ilmenite) crystallization.

Figures 3e,f,g,h show the behaviors of CaO, Na_2O , K_2O and P_2O_5 , respectively, in the residual melts of the hydrous experiments. The CaO LLD illustrates the effect of sub-calcic augite crystallization that begins shortly after pigeonite crystallization. Plagioclase crystallization in the lowest temperature experiments probably produces the final drop in CaO. Both Na_2O and K_2O behave as essentially incompatible elements throughout crystallization, steadily increasing in the residual melt with decreasing temperature. P_2O_5 generally increases throughout all experiments except the lowest temperature experiment. The P_2O_5 decrease in the lowest temperature experiment suggests that saturation of a P_2O_5 -bearing phase was achieved. Formation of a P_2O_5 -bearing phase in the most SiO_2 -rich melt of the hydrous LLD is in keeping with the findings of Harrison and

Table 3. Representative phase compositions.

Oxide	Pigeonite				Augite				Plagioclase		Magnetite		Ilmenite	
	MS-18	MS-51	MS-19	MS-52	MS-25	MS-51	MS-70	MS-52	MS-2b	MS-68	MS-1	MS-45	MS-30	MS-45
SiO ₂	52.92	50.27	53.03	49.31	48.24	50.59	50.92	49.37	56.18	55.40	—	—	—	—
Al ₂ O ₃	0.33	0.43	0.41	0.83	2.95	1.79	1.22	1.04	26.70	27.24	2.20	1.99	0.28	0.21
FeO*	18.73	30.29	19.99	29.98	18.28	13.52	16.98	21.99	1.15	1.23	80.72	69.40	47.40	47.04
MgO	21.19	13.61	21.23	11.77	13.49	14.03	14.00	9.90	—	—	2.56	1.26	2.34	1.94
CaO	4.88	4.36	4.30	6.26	13.01	18.47	14.96	14.95	10.11	11.05	—	—	—	—
Na ₂ O	0.03	0.04	0.06	0.07	0.34	0.23	0.15	0.14	4.95	4.49	—	—	—	—
TiO ₂	0.22	0.31	0.19	0.41	1.07	0.57	0.30	0.87	—	—	8.90	23.02	46.07	48.12
K ₂ O	—	—	—	—	—	—	—	—	0.16	0.24	—	—	—	—
MnO	0.76	0.52	0.68	0.46	0.67	0.44	0.50	0.52	—	—	0.66	0.26	0.64	0.53
	99.06	99.83	99.89	99.09	98.05	99.64	99.03	98.78	99.25	99.65	95.04	95.93	96.73	97.84

Watson (1984), who find that apatite saturation occurs at lower P₂O₅ contents in SiO₂-rich melts.

3.3. Dry Phase Assemblage and LLD

The PETMIX-calculated modes of the dry experiments are presented in Fig. 2b and representative phase compositions are contained in Table 3. At 1130°C, pigeonite (En₆₀Fs₃₁Wo₉) is the sole crystallizing phase and by 1080°C, sub-calcic augite (En₄₁Fs₂₇Wo₃₂) and plagioclase (An₄₉Ab₄₉Or₂ to An₅₃Ab₄₆Or₁) are also present in the assemblage. Small amounts of fayalite (~Fo₃₂) occur below 1065°C, Ti-magnetite has crystallized by 1050°C and at 1030°C, ilmenite is part of the phase assemblage. The TiO₂ content of magnetite increases until ilmenite begins to crystallize. The pyroxenes of each experiment except the 1130°C experiment contain some compositional zoning, likely developed by new pyroxene overgrowth onto preexisting pyroxenes. Pyroxene compositions are pictured Figure 5 and similar to the pyroxenes of the hydrous experiments, overlap pyroxene compositions comparable to those of Shergotty (Hale et al., 1999). No zoning was observed in plagioclase or olivine and no quench crystals were observed in any of the dry experimental products. A representative product of the dry experiments is shown in Figure 4b.

Fe loss and gain were taken into consideration for the experiments above 1080°C by allowing a pure Fe phase in the PETMIX calculations. The 1130°C experiment demonstrated Fe loss of ~3% and the 1080°C demonstrated Fe gain of ~2%.

Percentages of phases present other than the Fe phase were normalized to 100% and plotted in Figure 2.

The residual liquid compositions from the dry experiments are plotted in Figure 3 along with the A* starting composition and the residual liquid data from the hydrous experiments. Selected residual melt compositions are contained in Table 4. With decreasing temperature, melt SiO₂ in the dry experiments remains largely unchanged from the initial A* concentration until the lowest temperature (980°C) experiment (Fig. 3a). In the lowest temperature experiment, the crystallization of roughly three times more pyroxene, oxide and olivine than plagioclase leads to an increase in melt SiO₂. However, even after ~90% crystallization, the SiO₂ content of the residual liquid barely reaches the minimum SiO₂ content (56 wt%) for andesitic melt.

The Al₂O₃ contents of the dry experiment residual liquids follow a similar path to those of the hydrous experiments (Fig. 3b) In the experiments at 1080°C and below, Al₂O₃ increases despite the crystallization of plagioclase in most of the experiments. This continual increase in Al₂O₃ contrasts with the behavior demonstrated by the terrestrial dry LLD (Fig. 1a) which begins with a much higher Al₂O₃ basaltic starting material and crystallizes greater amounts of plagioclase. An explanation for the continual Al₂O₃ increase in the dry experiments lies in the changes in the mode from experiment to experiment. In the dry experiments, plagioclase crystallization begins in a low Al₂O₃ melt and the relative amounts of pla-

Table 4. Representative residual melt compositions.

Oxide	Hydrous experimental glasses						Dry experimental glasses						
	MS-18	MS-3b	MS-28	MS-38r	MS-30	MS-51	MS-19	MS-70	MS-68	MS-59	MS-56	MS-45	MS-52
SiO ₂	52.90	52.67	55.08	58.00	59.77	66.16	52.49	49.69	49.04	50.30	50.52	50.75	56.86
Al ₂ O ₃	8.18	9.73	10.69	10.88	12.92	11.74	8.99	9.97	10.22	10.28	9.47	9.78	11.11
FeO*	18.21	18.17	15.61	13.62	11.11	8.49	18.95	22.27	22.82	21.72	22.27	21.79	15.62
MgO	5.12	3.61	3.02	2.84	1.43	0.88	4.35	3.12	2.95	2.38	2.22	1.78	1
CaO	8.89	8.22	7.61	6.96	6.20	4.31	9.04	9.50	9.38	8.84	8.37	8.19	7.4
Na ₂ O	2.00	2.53	2.71	3.00	3.83	4.02	2.16	1.94	1.79	2.10	2.09	2.34	2.85
K ₂ O	0.59	0.63	0.70	0.76	1.02	1.63	0.62	0.50	0.47	0.77	0.95	1.04	1.64
TiO ₂	1.57	1.89	2.05	1.35	1.00	0.68	1.75	2.12	1.36	1.68	2.37	2.34	0.66
P ₂ O ₅	0.48	0.58	0.57	0.63	0.74	0.35	0.49	0.81	0.86	0.80	0.52	1.10	1.46
MnO	0.49	0.38	0.42	0.42	0.29	0.28	0.42	0.34	0.41	0.37	0.34	0.27	0.17
	98.44	98.44	98.46	98.47	98.31	98.54	99.26	99.31	99.31	99.24	99.13	99.38	98.77

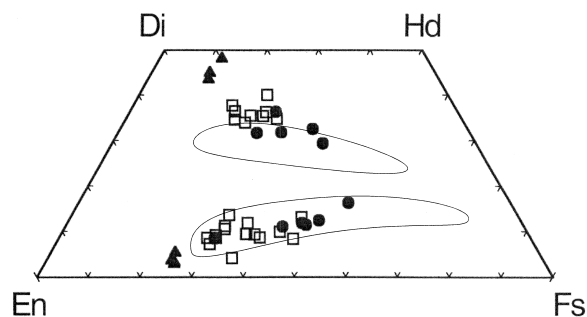


Fig. 5. Pyroxene compositions from the hydrous (open squares) and dry (filled circles) experiments of this study and analyses from the SNC meteorites Chassigny (filled triangles; Johnson et al., 1991) and Shergotty (Hale et al., 1999). The solid lines encompass Shergotty pyroxene compositions extrapolated from the data of Hale et al. (1999). The experimental pyroxene compositions extend between the compositions of Chassigny and Shergotty pyroxenes and continue to more Fe-rich compositions similar to those of the Shergotty pyroxenes.

gioclase and Al_2O_3 -poor phase (i.e. pyroxenes, oxides, olivine) crystallization remain in a roughly constant ratio of $\sim 26:74$ from 1050°C to 980°C . In the hydrous experiments, however, plagioclase crystallization begins later in a melt with higher Al_2O_3 and the proportion of plagioclase and Al_2O_3 -poor phases changes considerably. Between the 975°C and the 950°C experiments, the proportion of plagioclase to Al_2O_3 -poor phases changes from 14:86 to 24:76. This finding suggests that the increased proportion of Al_2O_3 -rich plagioclase in the mode of the hydrous experiments leads to a decrease in melt Al_2O_3 (Fig. 3b). Conversely, the constant predominance of Al_2O_3 -poor phases in the dry experiments prohibits Al_2O_3 from decreasing while plagioclase crystallizes.

The FeO contents of the dry LLD differ significantly from those of the hydrous melts (Fig. 3c). In the experiments at 1050°C and below, the combination of oxide, olivine, pyroxene and plagioclase crystallization leads to a slight decrease in melt FeO away from the maximum reached in the 1065°C experiment. In the lowest temperature experiment, the predominance of FeO-rich phases causes the melt FeO to decrease, but the LLD still remains well above the composition of the sulfur-free rock at the MgO content of the sulfur-free rock.

The behavior of melt TiO_2 in the dry LLD mimics that of the hydrous LLD but reaches a greater maximum in melt TiO_2 at a lower MgO value (Fig. 3d). TiO_2 increases in the residual melts during pyroxene-only crystallization, with the exception of the 1065°C experiment. The low TiO_2 content of the 1065°C experiment is not easily explained, but may be due to a combination of repeated use of the experimental starting material in previous experiments and small sample size. TiO_2 continues to increase in the 1050°C and 1030°C experiments despite the presence of magnetite \pm ilmenite in these experiments; this reflects the small amount of Ti-rich phases crystallizing in the 1050°C and 1030°C experiments. In the residual liquid of the 980°C experiment, which contains ilmenite as the dominant oxide, TiO_2 content is significantly reduced.

The behaviors of CaO, Na_2O , K_2O and P_2O_5 (Figs. 3e,f,g,h) in the dry experiments roughly parallel those of the residual melts of the hydrous experiments. A smaller decrease in CaO in the dry LLD relative to the hydrous LLD likely results from the

lesser amount of sub-calcic augite crystallization that occurs in the dry experiments (Fig. 2). Na_2O and K_2O again act as incompatible oxides with constantly increasing concentrations in the residual melts during crystallization. P_2O_5 also constantly increases throughout all of the dry experiments, indicating that phosphate saturation was not achieved. The absence of phosphate saturation in experiments with as little as 10% residual melt is likely due to the small degree of SiO_2 enrichment in the dry residual melts (Harrison and Watson, 1984).

4. DISCUSSION: SILICATE MELTS FROM SNC MAGMAS

4.1. Nature of the Problem

The identification of andesitic composition rocks at the Pathfinder site again raises the question of silicic magma genesis on Mars. It had been proposed that Mars, given the evidence for H_2O on the surface of the planet, would be intermediate between Earth and the Moon in terms of SiO_2 -rich magma abundance (Rutherford and Hess, 1981). The SNC meteorites contain evidence of SiO_2 -rich melts in the form of either late-stage mesostasis glasses or glasses within melt inclusions. Such glasses have been found in all of the 12 well-studied SNC meteorites (Kring and Gleason, 1998; Meyer, 1998). This widespread presence of quenched glasses with elevated SiO_2 contents suggests that derivation of andesitic igneous melts (and rocks) on Mars is possible on small scales. Questions remain, however, as to the conditions which produced these melts and whether the processes take place on a scale which would produce intrusions or eruptions of silicic magmas on Mars. Our primary experiments investigate the roles of water and starting composition in the development of the Mars Pathfinder sulfur-free rock composition, but are applicable to the development of Martian silicic magmas in general. Our experiments at varied water content and $f\text{O}_2$'s lend insight into the effects of these variables on the development of silicic magmas from characteristic Martian basalts, as well.

4.2. Fabrication of a SNC Basaltic Magma

The dry and hydrous pathways of SNC basalt crystallization investigated in this study produce different crystallization sequences over different temperature intervals. The order of crystallization in the hydrous experiments is pig \rightarrow aug \rightarrow mag \rightarrow plag + ilm \rightarrow ol (Fig. 2a), whereas the dry crystallization sequence is pig \rightarrow aug + plag + ol \rightarrow mag \rightarrow ilm. These differences are consistent with the expected effect of water on basalt crystallization and lead to significant differences between the LLD's produced by the two types of crystallization (Fig. 6). The potential for dry and hydrous SNC basalt crystallization pathways to create the sulfur-free rock, and other silicic compositions, can be evaluated using these LLD data. In the hydrous experiments, the early crystallization of magnetite exerts strong control on the behavior of SiO_2 , FeO and TiO_2 . The SiO_2 and FeO contents of the hydrous LLD reach those of the sulfur-free rock at the MgO content of the sulfur-free rock with $\sim 40\%$ to $\sim 60\%$ residual melt present (Figs. 2a and 6a,c). At the MgO content of the sulfur-free rock, the TiO_2 content of the hydrous LLD is generally higher than that of the sulfur-free rock, but the analytical error bars of the 975°C experiment do reach within the TiO_2 error bars of the sulfur-free rock (Fig.

6d). It should be noted that the A* starting composition has a higher TiO₂ content than most estimates of SNC parent melts (Table 1), and a starting material with slightly lower TiO₂ might produce a better match between the LLD and the sulfur-free rock. The Al₂O₃ content of the hydrous LLD reaches the Al₂O₃ content of the sulfur-free rock at ~30% crystallization and a higher MgO content than that of the sulfur-free rock (Figs. 2a and 6b). Stated another way, at the same MgO (2.0 wt%), the Al₂O₃ content of the LLD is higher than that of the sulfur-free rock. This suggests that with less suppression of plagioclase crystallization (less water), the hydrous LLD would be capable of reaching the Al₂O₃ content of the sulfur-free rock at the appropriate MgO. Alternatively, it is possible that the A* composition has a slightly higher Al₂O₃ content than the sulfur-free rock parent melt.

The oxides that display the greatest differences between the hydrous and dry LLD's are SiO₂ and FeO (Figs. 6a,c). At the MgO content of the sulfur-free rock, the SiO₂ content of the dry LLD falls well below the sulfur-free rock composition. Even in the lowest temperature experiment, which is 90% crystallized, the melt SiO₂ content did not reach the SiO₂ content of the sulfur-free rock (Fig. 6a). The FeO content of the dry LLD remains far above the FeO content of the sulfur-free rock (Fig. 6c), throughout the temperature interval investigated. As with SiO₂, greater than 90% crystallization would have to occur in order for the FeO content of the dry LLD to reach the sulfur-free rock FeO. The behavior of TiO₂ displays a similar difference between the dry and hydrous LLD's. The combination of later oxide crystallization and very small amounts of oxide crystallization in the dry experiments relative to the hydrous experiments prevents the dry LLD from reaching the SiO₂, FeO and TiO₂ contents of the sulfur-free rock. Although the dry LLD reaches the Al₂O₃ content of the sulfur-free rock at the MgO content of the sulfur-free rock, the importance of this is negated by the significant deviations of the SiO₂ and FeO contents of the dry LLD from the sulfur-free rock composition.

In summary, the hydrous LLD demonstrates that it is possible to produce a melt with the sulfur-free rock composition by the low-pressure crystallization of a SNC parent basalt which contains ~1.5 wt% dissolved H₂O. The hydrous residual melt reaches andesitic compositions (≥ 56 wt% SiO₂) with ~60% residual melt remaining and greater amounts of crystallization yield progressively more evolved magmas. Conversely, the dry, low-pressure LLD illustrates that crystallization of a SNC parent basalt under these experimental conditions fails to produce the sulfur-free rock composition, in agreement with the findings of McSween et al. (1999). The dry LLD does not reach the minimum SiO₂ content of andesitic magmas until only ~10% residual melt remains. The degrees of crystallization at which the hydrous and dry systems each reach andesitic melt compositions have implications for the physical separation of such melts. In the hydrous system, the larger melt fraction present when the residual melt reaches an andesitic composition would make it easier to either separate the melt from its coexisting crystals or mobilize the melt with entrained crystals for eruption onto the surface or intrusion into the Martian crust. At the stage where the residual melt becomes andesitic in the dry system, the small amount of residual melt present would likely inhibit melt movement and separation. The extraction of the dry andesite melt would be additionally hindered by its

higher viscosity. Thus, not only does ~1.5 wt% dissolved water allow a SNC parent basalt to fractionate to andesitic compositions, it increases the likelihood of producing a separate andesitic magma.

4.3. Effects of Reduced Water Contents

It is apparent from the results of the hydrous experiments that it is possible to produce melts with the andesitic compositions of the Mars Pathfinder rocks by crystallization of SNC basaltic magmas containing 1.5 wt% H₂O. We conducted a single experiment at QFM, 1030°C and $P_{\text{total}} = P_{\text{H}_2\text{O}} = 100$ bars to determine if SNC basaltic magmas with lesser amounts of water could still produce andesitic compositions like that of the sulfur-free rock. At 100 bars, water saturated basaltic melt contains ~1 wt% H₂O. The results of the single 100 bar experiment are plotted in Figure 6 relative to the 200 bar and dry LLD's. For the oxides shown, the residual melt of the 100 bar experiment falls within the trend delineated by the hydrous experimental products. This suggests that the SNC basalt phase equilibria at 100 bars are not significantly different from those at 200 bars, and that a SNC basaltic parent magma with only 1 wt% H₂O is also capable of producing andesitic melt compositions resembling the sulfur-free rock.

4.4. Effects of Different fO₂ Conditions

Understanding the effects of oxidation state on basalt crystallization is important because fO₂ affects which minerals crystallize from a basalt, especially Fe-Ti oxides (Spulber and Rutherford, 1983). By influencing the timing and abundance of Fe-Ti crystallization, oxidation state influences the potential of a magma to move to silicic compositions. The main set of experiments in this study was conducted at the QFM oxygen buffer. To explore the effect of different fO₂'s on the crystallization of a hydrous SNC basaltic parent magma, we conducted experiments on an initially QFM-buffered sample at more oxidizing (MnO-Mn₃O₄; MNO) and more reducing (graphite-methane; GCH) conditions. The MNO buffer is more oxidizing than any oxygen fugacity proposed for the SNC's (Delaney et al., 1998), but we selected it in order to clearly demonstrate the effects of more oxidizing conditions on basalt crystallization. The GCH buffer is slightly less reducing than the iron-wustite (IW) oxygen fugacity suggested by McSween et al. (1996) for QUE94201. The residual melt compositions of these experiments, both conducted at $P_{\text{total}} = P_{\text{H}_2\text{O}} = 200$ bars and 1030°C, are shown in Figure 6 relative to the dry and hydrous LLD's at QFM. Crystallization at the MNO buffer clearly led to a strong increase in melt SiO₂ and decreases in melt FeO and TiO₂ relative to the hydrous LLD at QFM. The SiO₂, FeO and TiO₂ contents of the MNO residual melt are explained by the more extensive crystallization of Fe-Ti oxides in this high fO₂ experiment. Large oxides are common in the experimental product and smaller oxides are present in the groundmass and frequently rim the pyroxenes. The MNO experiment is also considerably more crystallized (MgO ~ 0.8 wt%) relative to an experiment at QFM and 1030°C (MgO ~ 2 wt%). The greater degree of crystallization in the MNO experiment can be attributed to the effective increase in the

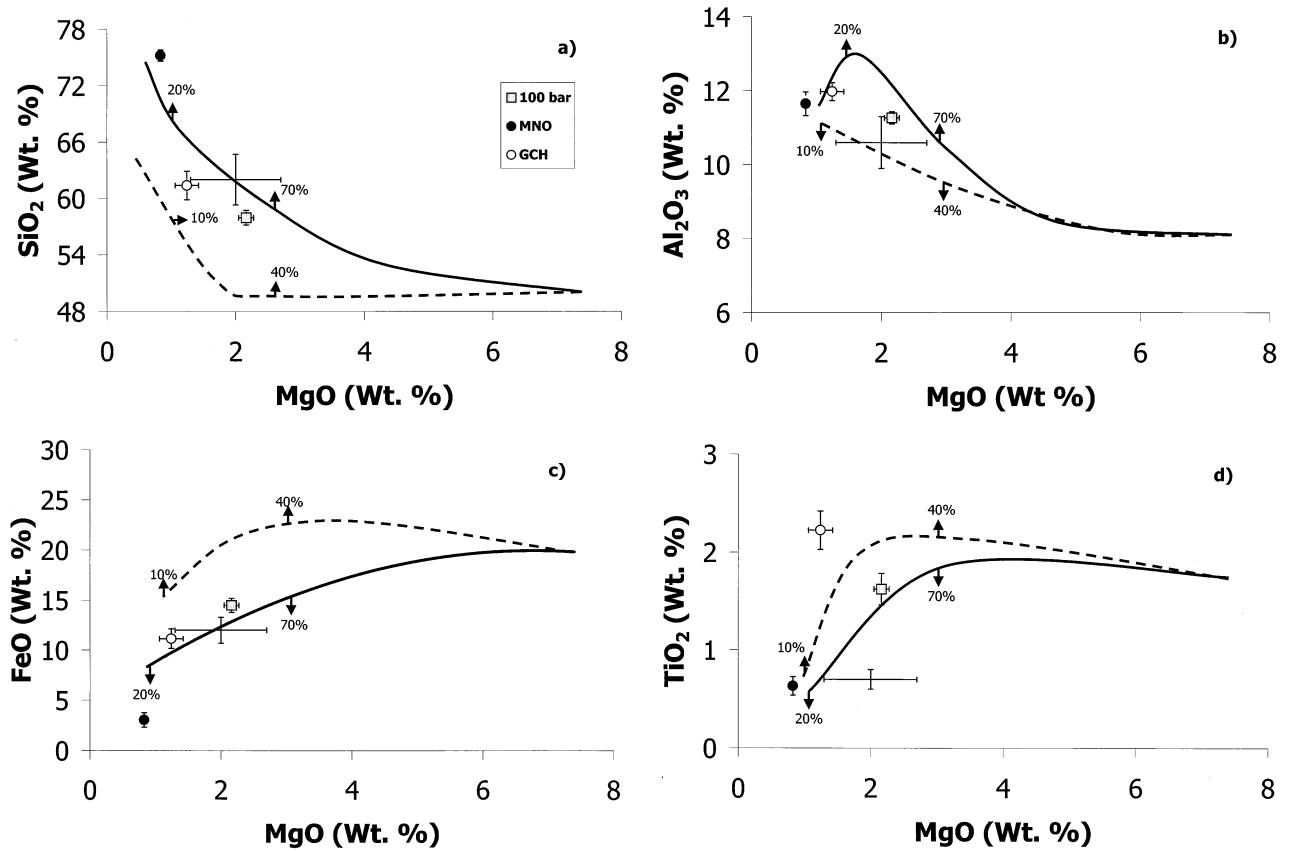


Fig. 6. Additional experimental data demonstrating the effects of varied water contents and oxygen fugacities on the crystallization of A*. The lines are fit to the data of Figure 3 and schematically represent the hydrous and dry LLD's constructed at QFM: the solid line is the 200 bar hydrous LLD and the dashed line is the dry LLD. Labeled arrows along the LLD's indicate the amount of residual liquid present in different experiments along the LLD's. The square symbol represents the product of the 100 bar experiment, the filled circle represents the MnO-Mn₂O₄ buffered experiment (equivalent to QFM + 3) and the open circle represents the graphite-methane buffered experiment (equivalent to QFM - 3). Error bars for all points encompass $\pm 1\sigma$. The cross marking the sulfur-free rock composition delineates the analytical uncertainties in the APXS measurements (Brückner et al., 1999).

Mg# of silicates in the experiment caused by Fe²⁺ oxidation and oxide crystallization.

The residual melt of the GCH experiment has a lower SiO₂ content and higher FeO and TiO₂ content relative to the hydrous QFM LLD at the same MgO. The composition of the GCH residual melt reflects the small amount of oxide crystallization observed in the product (~2%; optically determined) relative to QFM. Reducing conditions at GCH discourage oxide crystallization and in turn, decreased oxide crystallization decreases the degree of SiO₂ enrichment experienced by the crystallizing basalt. As in the MNO-buffered sample, the MgO content of the GCH experimental product is lower (MgO ~ 1.2 wt%) than that of a QFM experiment at the same temperature. The high P_{H₂} produced by the GCH buffer reduces the P_{H₂O} of the experiment to ~130 bars which effectively increases the amount of crystallization that occurs at 1030°C and decreases the MgO content of the experimental product. Overall, conditions more oxidizing than those of the QFM buffer will cause a hydrous crystallizing SNC parent basalt to reach evolved residual melt compositions earlier in the LLD, whereas conditions more reducing than those of the QFM

buffer tend to prevent the development of evolved residual melts.

4.5. Source of Water in Martian Basalt Fractionation

Invoking water in the formation of rocks such as the Mars Pathfinder sulfur-free rock is supported by evidence for the presence and action of water on Mars at macroscopic and microscopic levels. The Mariner and Viking missions of the 1970's provided the first indication that flowing water may have created morphologic features on the Martian surface. Dendritic valley networks in the southern hemisphere highlands and outflow channels extending from the highlands to the low plains of the northern hemisphere imply that the climate on Mars might have been suitable at one time for the existence of liquid water on its surface (e.g. Sagan et al., 1973a). The recognized importance of the action of water on the surface of Mars was highlighted by the selection of Ares Vallis, a channel carved by catastrophic floods (Golombek, 1997), as the landing site for the Mars Pathfinder mission.

At the microscopic level, studies of the SNC meteorites have

revealed that a subset of SNC meteorites contain kaersutite- and biotite-bearing melt inclusions (e.g. Floran et al., 1978; Johnson et al., 1991). These phases were used to arrive at the value of 1.5 wt% H₂O in SNC melts (e.g. Johnson et al., 1991). While the cause of the low water contents measured in these phases by Watson et al. (1994) is yet undetermined, it is not unreasonable to presume water might play a role in Martian basalt crystallization at depth in the crust.

Our experiments show that the presence of as little as 1 wt% dissolved water in a crystallizing Martian basalt allows the basalt to fractionate to andesitic residual melt compositions, most notably the composition of the sulfur-free rock. If this did occur, an essential issue is how water could become incorporated into a Martian magma. We consider that there are basically three different pathways for the creation of hydrous basaltic magmas on Mars: melting of water-bearing mantle and H₂O buildup during fractionation; assimilation of hydrothermally altered materials into a basalt; and direct introduction of water from a hydrothermal system into a magma body.

Currently, little agreement exists regarding the water content of the Martian mantle, making it difficult to constrain the water contents of magmas derived from the mantle. Dreibus and Wänke (1987) propose one of the lowest estimates, suggesting that 36 ppm of H₂O remained in the mantle after H₂O reacted with Fe metal during the formation of Mars. Mysen et al. (1998) also estimated low mantle water contents based on the low water contents of the SNC amphiboles; however, their estimate was based on the assumption that the SNC amphiboles had undergone no post-crystallization dehydrogenation. This assumption is called into question by results from King et al. (1999) which demonstrate that terrestrial amphiboles undergo dehydrogenation during ascent. There does not appear to be an agreed upon upper limit to the amount of water in the Martian mantle in the literature, but McSween and Harvey (1993) offer a possible scenario that would create a wetter Martian mantle. According to McSween and Harvey (1993), it is possible that the reduction of H₂O by Fe metal proposed by Dreibus and Wänke (1987) was not a completely efficient process. If only 2% of the original Martian water budget was left unreacted, ~700 ppm of water would have remained in the mantle after core formation (Carr, 1996). Regardless of the Martian mantle water content, we do not expect the mantle to yield a primary mantle melt with 1.5 wt% H₂O. Thus, in addition to the water introduced into a melt from partial melting of the mantle, crystal fractionation of anhydrous minerals is necessary to increase the water concentration of a mantle melt to ~1.5 wt%. Evidence of the accumulation of anhydrous minerals is provided by the SNC's, many of which contain evidence of an active crystal accumulation process (McSween, 1994). Assuming a melt created by 10% melting of the mantle and complete incompatibility of H₂O in mantle residue, extensive (>95%) fractional crystallization would be required to reach 1.5 wt% H₂O in a melt from mantle with 36 ppm H₂O. A 10% partial melt of mantle with 700 ppm H₂O, however, would only require ~50% fractional crystallization in order to produce a melt with 1.5 wt% H₂O.

Terrestrially, stoping or assimilation of hydrothermally altered wall rocks has been used to explain the existence of ¹⁸O-depleted magmas (Gunnarsson et al., 1998) in a region (Iceland) of mantle-derived magmas. Evidence of both assim-

ilation and hydrothermal alteration processes, which together could ultimately produce a hydrous basaltic magma, is present within the SNC's. Assimilation has been called upon to reconcile the REE contents and Sm-Nd isotopic compositions of Shergotty and Zagami (Longhi, 1991). Both Shergotty and Zagami have LREE-depleted patterns and $-\epsilon_{Nd}$ isotopic compositions, signatures not expected in a single product of a simple melting process (Faure, 1986). Longhi (1991) suggested that assimilation of crustal material with long term LREE enrichment (and therefore $-\epsilon_{Nd}$) by a basalt derived from a LREE-depleted source could account for both the LREE and isotopic composition of Shergotty and Zagami. Evidence of minor ($\leq 3\%$) hydrothermal alteration of near surface rocks on Mars is provided by various secondary minerals (iddingsite, carbonate) in the SNC meteorites (Treiman et al., 1993; Wadhwa and Crozaz, 1994). It is possible that more heavily altered rocks exist in the subsurface Martian crust which would contribute sufficiently large quantities of water to a magma. For the magma to dissolve the necessary 1–1.5 wt% H₂O, assimilation would have to occur at depth (~1 km) where the pressure is ≥ 100 bars. Evidence of more heavily weathered rocks may also be lacking among the SNC meteorites because such rocks may not survive the impact process sufficiently intact to escape Mars.

Groundwater reservoirs have been suggested for Mars largely in order to explain the extensive landforms attributed to flowing water at the surface (Clifford, 1993). It has also been proposed that water contained within groundwater reservoirs could be mobilized in response to the presence of a magma body thus establishing a hydrothermal system (Gulick, 1992). Such a hydrothermal system might be capable of introducing water into the magma. This process is likely difficult in light of the relative rates of magma cooling and water diffusion as outlined by Taylor and Sheppard (1986). However, Hildreth et al. (1984) and Sheppard and Harris (1985) proposed that water could be directly injected into a magma during a caldera collapse event. This process entails drawing of water from a surrounding hydrothermal system into a decompressing magma chamber during caldera collapse and magma extrusion. Water would then become incorporated into the remaining magma after the eruption process ceased. While Hildreth et al. (1984) and Sheppard and Harris (1985) invoked the injection of water into magma during caldera collapse to explain characteristics of rhyolitic systems on Earth, this process is still relevant to Mars. Caldera features are found on all four Tharsis volcanoes (Carr, 1973) and are frequently found on patera (Greeley and Spudis, 1981). Thus, incorporation of water into a magma on Mars during caldera collapse is feasible and could ultimately create a hydrous basalt capable of fractionating to more evolved compositions.

Invoking the action of water in the formation of the Mars Pathfinder sulfur-free rock also leads to the question of the fate of that water. One possibility is that the water was degassed during ascent to the surface of either the andesitic magma or the magma and incorporated crystals that became the sulfur-free rock. Degassing during ascent has been used to explain the overall dry nature of the SNC meteorites despite the presence of hydrous minerals within melt inclusions (McSween, 1994). A second possibility is that some or all of the water remained within the rock. This would be less likely for effusively erupted

magmas, but might occur in the case of intrusives. The amount of water proposed in the formation of the sulfur-free rock, 1–1.5 wt% H₂O, is insufficient for the formation of hydrous minerals such as amphibole and mica from a melt. However, water segregated interstitially could become incorporated into late-stage, interstitial hydrous minerals. Such a late-stage, interstitial fluid could produce the type of alteration seen in the SNC meteorites (e.g. Treiman et al., 1993) or could lead to the formation of hydrous weathering products in the Martian soil, such as ferrihydrite (McSween et al., 1999). Unfortunately, if water were still present in the sulfur-free rock, the APXS could not detect it as it is not capable of detecting H (Rieder et al., 1997).

5. CONCLUSION

The results of this experimental study reveal that a residual melt equal to the Mars Pathfinder sulfur-free rock, classified as an andesitic igneous rock, can be produced through crystallization of a hydrous SNC parent basalt (high FeO, low Al₂O₃) at the QFM oxygen buffer. In contrast, crystallization of a dry SNC parent basalt does not produce melts equivalent to the sulfur-free rock. The fundamental difference between the hydrous and dry basalt crystallization paths is produced by timing and amount of Fe-Ti oxide crystallization. Water facilitates early crystallization of Fe-Ti oxides which leads to early increases in residual melt SiO₂ and decreases in residual melt FeO and TiO₂. SiO₂ enrichment produced through oxide crystallization allows hydrous SNC basaltic melt to fractionate to andesitic melt compositions. Andesitic residual melt compositions are produced in the hydrous suite of experiments after ~40% crystallization and reach SiO₂-rich andesite compositions (SiO₂ = 62%) after ~65% crystallization. Water concentrations as low as 1 wt% are capable of directing the crystallization path of a SNC parent basalt to andesitic residual melt compositions. The fact that SiO₂-enriched residual melts are produced after only ~40% crystallization of a hydrous SNC basalt makes it much more likely that such a residual melt could be separated from crystals and erupted from or intruded into the Martian crust. In the dry experiments, late and sparse crystallization of oxides delays SiO₂ enrichment of the SNC parent basalt until much of the basalt has crystallized (~90%). Experiments conducted at other oxygen fugacities reveal that conditions more oxidizing than QFM encourage earlier formation and hence physical separation of SiO₂-enriched liquids while conditions more reducing than QFM hinder their formation. Invoking water in the formation of the sulfur-free rock is considered reasonable in light of the extensive evidence for the action of water on the surface of Mars and the evidence of magmatic water provided by the SNC meteorites. Various pathways of introduction of water into a magma are feasible on Mars including melting of water-bearing mantle followed by fractional crystallization of anhydrous minerals, assimilation of hydrothermally altered materials into a magma and direct introduction of water from a hydrothermal system into a magma during caldera collapse.

Acknowledgments—This research was supported by NASA grants NAG5-4438 and NAG5-8181 to MJR. The authors wish to thank Hap McSween, Gerlind Dreibus-Kapp and Connie Bertka for their insight-

ful reviews. We also wish to thank Dr. Joseph Devine for assistance with electron microprobe analyses and PETMIX calculations.

REFERENCES

- Brückner J., Dreibus G., Lugmair G. W., Rieder R., Wänke H., and Economou T. (1999) Chemical composition of the Martian surface as derived from Pathfinder, Viking and Martian meteorite data. In *LPSC 30*, Abstract #1250, Lunar and Planetary Institute, Houston (CD-ROM).
- Carmichael I. S. E. (1964) The petrology of Thingmuli, a Tertiary volcano in eastern Iceland. *J. Petrol.* **5**, 3, 435–460.
- Carr M. H. (1973) Volcanism on Mars. *J. Geophys. Res.* **78**, 20, 4049–4062.
- Carr M. H. (1996) *Water on Mars*. Oxford University Press.
- Carroll M. R. and Webster J. D. (1994) Solubilities of sulfur, noble gases, nitrogen, chlorine, and fluorine in magmas. In *Reviews in Mineralogy* (eds. M. R. Carroll and J. R. Holloway), Vol. 30, pp. 231–279. Mineralogical Society of America.
- Clifford S. M. (1993) A model for the hydrologic and climatic behavior of water on Mars. *J. Geophys. Res.* **98**, E6, 10973–11016.
- Delaney J. S., Sutton R. S., and Dyar M. D. (1998) Variable oxidation states of iron in Martian meteorites. In *LPSC 29*, Abstract #1241, Lunar and Planetary Institute, Houston (CD-ROM).
- Dreibus G. and Wänke H. (1987) Volatiles on Earth and Mars: A comparison. *Icarus* **71**, 225–240.
- Faure G. (1986) *Principles of Isotope Geology*. John Wiley & Sons.
- Floran R. J., Prinz M., Hlava P. F., Keil K., Nehru C. E., and Hinthorne J. R. (1978) The Chassigny meteorite: A cumulate dunite with hydrous amphibole bearing melt inclusions. *Geochim. Cosmochim. Acta* **42**, 1213–1229.
- Ghiorso M. S. and Sack R. O. (1995) Chemical mass transfer in magmatic processes, IV.: A revised and internally consistent thermodynamic model for the interpolation and extrapolation of liquid-solid equilibria in magmatic systems at elevated temperatures and pressures. *Contrib. Mineral. Petrol.* **119**, 197–212.
- Ghosal S., Sack R. O., Ghiorso M. S., and Lipschutz M. E. (1998) Evidence for a reduced, Fe-depleted martian mantle source region of shergottites. *Contrib. Mineral. Petrol.* **130**, 346–357.
- Golombek M. P. (1997) The Mars Pathfinder mission. *J. Geophys. Res.* **102**, E2, 3953–3965.
- Greeley R. and Spudis P. (1981) Volcanism on Mars. *Rev. Geophys. Space Phys.* **19**, 13–41.
- Gulick V. C. (1992) Magmatic intrusions and hydrothermal systems on Mars. *Lunar Planet. Inst. Tech. Rept.* **92-02**, 50–51.
- Gunnarsson B., Marsh B. D., and Taylor H. P. Jr. (1998) Generation of Icelandic rhyolites: silicic lavas from the Torfajökull central volcano. *J. Volcanol. Geotherm. Res.* **83**, 1–45.
- Hale V. P. S., McSween H. Y. Jr., and McKay G. A. (1999) Re-evaluation of intercumulus liquid composition and oxidation state for the Shergotty meteorite. *Geochim. Cosmochim. Acta* **63**, 9, 1459–1470.
- Harrison T. M. and Watson E. B. (1984) The behavior of apatite during crustal anatexis: Equilibrium and kinetic considerations. *Geochim. Cosmochim. Acta* **48**, 1467–1477.
- Hildreth W., Christiansen R. L., and O'Neil J. R. (1984) Catastrophic isotopic modification of rhyolitic magma at times of caldera subsidence, Yellowstone Plateau volcanic field. *J. Geophys. Res.* **89**, 8339–8369.
- Johnson M. C., Rutherford M. J., and Hess P. C. (1991) Chassigny petrogenesis: Melt compositions, intensive parameters, and water contents of Margan (?) magmas. *Geochim. Cosmochim. Acta* **55**, 349–366.
- Juster T. C., Grove T. L., and Perfit M. R. (1989) Experimental constraints on the generation of FeTi basalts, andesites, and rhyodacites at the Galapagos Spreading Center, 85°W and 95°W. *J. Geophys. Res.* **94**, 9251–9274.
- King P. L., Hervig R. L., Holloway J. R., Vennemann T. W., and Righter K. (1999) Oxy-substitution and dehydrogenation in mantle-derived amphibole megacrysts. *Geochim. Cosmochim. Acta* **63**, 21, 3635–3651.
- Kring D. A. and Gleason J. D. (1998) Siliceous igneous rocks on Mars.

- In *Lunar Planet. Sci.* **30**, Abstract #1611, Lunar and Planetary Institute, Houston (CD-ROM).
- Longhi J. (1991) Complex magmatic processes on Mars: Inferences from the SNC meteorites. *Proc. Lunar Planet. Sci. Conf.* **21**, 695–709.
- McSween H. Y. Jr. (1994) What we have learned about Mars from SNC meteorites. *Meteoritics* **29**, 757–779.
- McSween H. Y. Jr. and E. Jarosewich (1983) Petrogenesis of the Elephant Moraine A79001 meteorite: multiple magma pulses on the shergottite parent body. *Geochim. Cosmochim. Acta* **47**, 1501–1513.
- McSween H. Y. Jr. and Harvey R. (1993) Outgassed water on Mars: Constraints from melt inclusions in the SNC meteorites. *Science* **259**, 1890–1892.
- McSween H. Y. Jr., Eisenhour D. D., Taylor L. A., Wadhwa M., and Crozaz G. (1996) QUE94201 shergottite: Crystallization of a Martian basaltic magma. *Geochim. Cosmochim. Acta* **60**, 22, 4563–4569.
- McSween H. Y. Jr. et al. (1999) Chemical, multispectral, and textural constraints on the composition and origin of rocks at the Mars Pathfinder landing site. *J. Geophys. Res.* **104**, E4, 8679–8715.
- Meyer C. (1998) Mars Meteorite Compendium—1998. Office of the Curator, Johnson Space Center.
- Miniti M. E., Rutherford M. J., and Watson B. E. (1999) The effect of impact shock on the water content and H isotopic composition of hornblende: Applications to the SNC meteorites. *EOS Trans.* **80**, 46, F596 (abstr.).
- Mysen B. O., Virgo D., Popp R. K., and Bertka C. M. (1998) The role of H₂O in Martian magmatic systems. *Am. Mineral.* **83**, 942–946.
- Nielsen C. H. and Sigurdsson H. (1974) Quantitative methods of electron microprobe analysis of sodium in natural and synthetic glasses. *Am. Mineral.* **66**, 547–552.
- Popp R. K., Virgo D. and Phillips M. W. (1995a) H deficiency in kaersutitic amphiboles: Experimental verification. *Am. Mineral.* **80**, 1347–1350.
- Rieder R., Economou T., Wänke H., Turkevich A., Crisp J., Brückner J., Dreibus G., and McSween H. Y. Jr. (1997) The chemical composition of Martian soil and rocks returned by the mobile alpha proton X-ray spectrometer: Preliminary results from the X-ray mode. *Science* **278**, 1771–1776.
- Rutherford M. J. and Hess P. C. (1981) Granite genesis in a planetary context: Processes and important variables for Mars. *LPSC* **12**, 915–917 (abstr.).
- Sagan C., Toon O. B., and Gierasch P. J. (1973a) Climate change on Mars. *Science* **181**, 1045–1049.
- Sheppard S. M. F. and Harris C. (1985) Hydrogen and oxygen isotope geochemistry of Ascension Island lavas and granites: Variation with crystal fractionation and interaction with sea water. *Contrib. Mineral. Petrol.* **91**, 74–81.
- Spulber S. D. and Rutherford M. J. (1983) The origin of rhyolite and plagiogranite in oceanic crust: An experimental study. *J. Petrol.* **24**, 1, 1–25.
- Stolper E. and McSween H. Y. Jr. (1979) Petrology and origin of the shergottite meteorites. *Geochim. Cosmochim. Acta* **43**, 1475–1498.
- Taylor H. P. Jr. and Sheppard S. M. F. (1986) Igneous rocks: I. Processes of isotopic fractionation and isotope systematics. In *Reviews in Mineralogy* (eds. J. W. Valley, H. P. Taylor Jr., and J. R. O'Neil), Vol. 16, pp. 227–271. Mineralogical Society of America.
- Treiman A. H. (1993) The parent magma of the Nakhla (SNC) meteorite, inferred from magmatic inclusions. *Geochim. Cosmochim. Acta* **57**, 4753–4767.
- Treiman A. H., Barrett R. A. and Gooding J. L. (1993) Preterrestrial aqueous alteration of the Lafayette (SNC) meteorite. *Meteoritics* **28**, 86–97.
- Wadhwa M. and Crozaz G. (1994) Constraints on the rare earth element characteristics of metasomatizing fluids in the martian meteorite ALH84001. *LPSC* **26**, 1451–1452 (abstr.).
- Watson L. L., Hutcheon I. D., Epstein S., and Stolper E. M. (1994) Water on Mars: Clues from deuterium/hydrogen and water contents of hydrous phases in SNC meteorites. *Science* **265**, 86–90.
- Wright T. L. and Doherty P. C. (1970) A linear programming and least squares computer method for solving petrologic mixing problems. *Bull. Geol. Soc. Amer.* **81**, 1995–2008.